

**Projected changes in both mean climate and climate variability drive substantial  
increases in extreme fire weather in the western United States**

Danielle Touma<sup>a,b</sup> & Clara Deser<sup>b</sup>

<sup>a</sup> *Jackson School of Geosciences, Institute for Geophysics, University of Texas at Austin, Austin, TX*

<sup>b</sup> *Climate and Global Dynamics, National Center for Atmospheric Research, Boulder, CO, USA.*

*Corresponding author:* Danielle Touma, [danielle.touma@utexas.edu](mailto:danielle.touma@utexas.edu)

## ABSTRACT

Wildfire frequency, extent and duration in the western United States (U.S.) are projected to increase throughout the 21st century as dry and warm conditions become more frequent, widespread, and persistent. However, there is limited knowledge about how changes in mean climate and changes in climate variability, individually and together, contribute to these increases. To disentangle these effects, we use a 100-member ensemble of climate simulations produced with the Community Earth System Model v2 under historic and SSP3-7.0 forcing from 1980-2100. Using the Canadian Forest Fire Weather Index (FWI) to quantify fire-related meteorological conditions in the simulations, we select extreme FWI thresholds relative to a baseline distribution centered at 1980 (“fixed threshold”) and an evolving distribution (“moving threshold”) to identify spatiotemporally connected extreme fire weather events. By 2100, the frequency, area, and number of event days increase when considering a fixed threshold, and events are up to 4°C warmer on average. Moreover, events over the Pacific Coast expand northwestwards, while those over the Four Corners region expand westwards and northeastwards. Changes in event frequency are small and not significant when considering a moving baseline but become spatiotemporally more connected and widespread, reflecting non-thermodynamically driven changes. Increases in the mean of maximum temperature, as well as changes in both the variability and mean of relative humidity, drive the largest increases in extreme fire weather event area and number of event days. By quantifying how changes in the mean and variability of climate variables impact wildfire conditions in the western U.S., our study has implications for increasing resiliency to wildfire risk under climate change.

## 1. Introduction

Wildfires in recent years have become more synchronous, occurring in different parts of the North American continent simultaneously, and compounding the impacts felt in the region (Abatzoglou et al. 2021). For example, in 2023, unprecedented wildfires Canada were burning from east to west across the country simultaneously, straining the capacity for coordinated firefighting and leading to poor air quality in much of the United States (U.S.) and Canada (Jones et al. 2024; Kirchmeier-Young et al. 2024). Similarly, in 2020, the western U.S. experienced widespread wildfire activity – while the number of fires was in the normal historic range, the burn area and the number of very large fires were the highest recorded, leading to 40 fatalities and US\$20 billion in losses. Moreover, in much of the

western U.S., wildfire area and severity have increased over the last few decades (Jones et al. 2022). Specifically, increases in the total burned area and the number of large wildfires have been attributed to anthropogenically-forced anomalous warming and drying in recent years (Jain et al. 2022; Juang et al. 2022; Abatzoglou et al. 2025) and over a century of forest fire suppression (Andela et al. 2017; Jones et al. 2022; Hagmann et al. 2021). The damages felt by society due to these increases in wildfire area have also risen, with larger populations and more resources being exposed to wildfire hazards (Burke et al. 2021). Moreover, these larger and more frequent wildfires have exacerbated populations' exposure to smoke and post-fire hydrologic hazards, such as debris flows and channel sedimentation (Oakley 2021). These impacts have both short term and long term impacts on hydrology (Collar et al. 2022; Williams et al. 2022), livelihoods (Lawrence et al. 2022), and public health (Burke et al. 2021).

Many studies have assessed trends in fire weather conditions – dry, warm and windy conditions – using fire weather indices such as the Canadian Forest Fire Weather Index (FWI) and the McArthur Forest Fire Danger index (FFDI), and their impact on the likelihood, frequency, and area of wildfires in recent years. Observed increases in extreme fire weather events lead to increases in burned forest area and higher frequency of large wildfires globally and in the western U.S. (Abatzoglou and Williams 2016; Goss et al. 2020; Jain et al. 2022; Jones et al. 2022). These increases largely stem from increases in maximum temperature and decreases in relative humidity prior to and during wildfire seasons, and have been linked to an increase in the frequency and intensity of atmospheric ridging in the northeast Pacific Ocean (Sharma et al. 2022). The southwest U.S. has also been impacted by “failed” North American monsoon seasons as well as delays in monsoon onsets, leading to longer-than-usual dry conditions and subsequently higher wildfire activity (Cook and Seager 2013; Hoell et al. 2022). Changes in these conditions across the western U.S. are largely driven by increases in global greenhouse gas emissions and localized reductions in aerosol emissions (Abatzoglou and Williams 2016; Kirchmeier-Young et al. 2017; Touma et al. 2021). In future years, projected increases in greenhouse gas emissions and continued reductions in aerosol emissions are expected to lead to further increases in frequencies and durations of extreme fire weather conditions, leading to higher risks of wildfires, and causing the frequency of extreme fire weather conditions to emerge well beyond the expected historic frequency, with fire weather conditions reaching a “new normal” by the end of the 21<sup>st</sup> century (Abatzoglou et al. 2019; Touma et al. 2021, 2022).

Several studies have used large ensemble Earth System Model (ESM) simulations to quantify the trends in fire weather conditions in future climate projections. There is a large consensus that fire weather conditions are projected to increase over much of the globe when accounting for both model discrepancies (Abatzoglou et al. 2019; Bui et al. 2024) and irreducible internal variability (Kirchmeier-Young et al. 2017; Touma et al. 2021). Given systemic biases in ESMs, especially in the representation of the FWI (Gallo et al. 2023; Touma et al. 2021) and the driving variables (Fasullo, 2020; Simpson et al., 2024), the general approach is to use upper tails of the FWI distribution to define “extreme” fire weather within each ESM.

Here, we compare the more traditional choice of using “fixed” historic or pre-industrial distributions of fire weather indices to calculate upper-tail thresholds to describe “extreme” fire weather conditions to the choice of using a moving-window threshold (hereafter, “moving threshold”), which captures the time-evolving distribution of fire weather conditions. In recent marine heat wave literature, it has been argued that using a fixed baseline can obscure local and short-term drivers of these extremes in future scenarios due to the saturation of marine heat wave occurrences caused by a warming climate (Smith et al. 2025; Capotondi et al. 2024; Deser et al. 2024). For terrestrial heatwaves, studies have compared changes in heatwaves defined using a moving baseline to those using a fixed baseline to separate thermodynamic from non-thermodynamic effects on changes in heatwave area and duration (Skinner et al. 2025; Vogel et al. 2020). Using a moving threshold can also reveal additional criteria for adaptation measures needed to overcome changes in extreme climate events, beyond those driven by mean changes alone (Amaya et al. 2023). In our study, a moving threshold would ensure that the frequency of fire weather days for a specific location remain constant through time, however, the intensity and area of events could still change through changes in the variability beyond the extreme threshold. Moreover, spatial or temporal clustering or connectivity of extreme fire weather events could also increase, due to non-thermodynamic changes. This could lead to greater spatially compounding risks with multiple wildfires occurring simultaneously or in succession, resulting in increased burned area, greater smoke exposure from wildfire emissions, and the preconditioning of larger areas to post-fire hydrologic hazards (Raymond et al. 2020; Zscheischler et al. 2020).

Few studies have assessed how changes in the variability of the climate system, and not just the mean of the climate, has impacted wildfire risk under anthropogenic forcing. By

doing so, changes in the variability are assumed to be negligible or part of the “noise” of our climate system – however, this could lead to the underestimation of the impact of anthropogenic forcing on wildfire risk. Zhuang et al. (2021) found that changes in atmospheric circulation, or natural variability, explained one-third of the observed vapor pressure deficit increase over the western U.S. in recent decades. While their study leveraged multi-model simulations from the CMIP6 archive, single-model initial-condition large ensembles could provide a more robust estimate of these influences by overcoming uncertainties from model physics (Deser et al. 2020; Zhuang et al. 2021).

In this study, we use the 100-member Community Earth System Model v2 Large Ensemble (CESM2-LE) to assess projected changes under SSP3-7.0 (Rodgers et al. 2021) in the Four Corners (Utah, Colorado, New Mexico and Arizona) and the Pacific Coast (California, Oregon and Washington) regions, which have been experiencing increasing trends in large and severe wildfires (Abatzoglou et al. 2025). We show how extreme fire weather events respond to anthropogenic climate change in terms of their frequency, number of event days, area, and intensity during the height of the western U.S. fire season, June to October (JJASO). We address two main research gaps in understanding wildfire risk in the western U.S. First, we use both a fixed and moving-window period to calculate location-specific extreme percentile thresholds and identify spatiotemporally connected grid points as extreme fire weather events. By using these two types of thresholds, we disentangle the thermodynamic drivers of changes in extreme fire weather events from other non-thermodynamic drivers and provide insight on fire-related adaptation needs in these regions. Secondly, through the development of a novel framework, we isolate the effects of changes in the mean and variability of climate drivers on changes in the number of event days, area, frequency and intensity of these events. This allows new insight into how changes in climate variability, in addition to changes in the mean climate, will influence wildfire risk.

## **2. Data and Methods**

### *a. CESM2-LE simulations*

We use the CESM2-LE simulations to quantify historic and future fire weather. As demonstrated in previous studies (e.g., Kirchmeier-Young et al., 2017; Touma et al., 2021, 2022), using a large ensemble allows robust assessment of changes in extreme fire weather events under anthropogenic forcing as well as internal variability. The CESM2-LE consists of

100 members and has daily resolution data publicly available, making it a unique and unprecedented dataset to understand future projections of extreme fire weather events.

The CESM2 model is a fully coupled atmosphere, ocean, land, and sea-ice model on a nominal 1-degree grid. The 100 members of the CESM2-LE are simulated under historic (1850-2014) and SSP3-7.0 (2015-2100) scenarios (Rodgers et al. 2021). The SSP3-7.0 scenario has both high greenhouse gases and aerosol emissions – this was chosen for the CESM2-LE in order to enable the detection and quantification of forced changes in the mean and natural variability (Rodgers et al. 2021), making it suitable for our study. The ensemble members are initialized through a combination of macro and micro perturbations, where macro perturbations are introduced using different Atlantic Meridional Overturning Circulation (AMOC) states, and micro-perturbations are introduced using a random perturbation to the atmospheric temperature field (Rodgers et al. 2021). The memory of the initial conditions is lost within a few decades (Deser et al. 2025). We note that all 100 members use identical forcing, except for the biomass burning aerosols. Half of the members follow the Coupled Model Intercomparison Project Phase 6 (CMIP6) protocol for biomass burning, which consists of low-pass filtered (11-year smoothing) timeseries except over the period 1990-2020 when high-frequency satellite-based measurements are available (Van Marle et al. 2017). This introduces a discontinuity in temporal variance of biomass burning aerosols, which in turn has been shown to produce a rectified effect on climate conditions over high northern latitudes in association with Arctic sea ice feedbacks (e.g., DeRepentigny et al., 2022). For this reason, the other half of the members use 11-year smoothed biomass burning timeseries over the entirety of the simulations (see Rodgers et al. 2021 for additional information). We find no discernable differences between the two halves of the CESM2-LE members for our analysis and therefore consider all 100 members together.

#### *b. Canadian Forest Fire Weather Index (FWI)*

The Canadian Forest Fire Weather Index System (CFFWIS) consists of three moisture codes and three fire behavior indices and was empirically derived by Van Wagner (1987). The Fire Weather Index (FWI) itself, which is part of the CFFWIS, is a numeric rating of fire intensity and accounts for the moisture codes and other indices in the system, and its calculation is described in Dowdy et al. (2009). FWI is widely used, both operationally and in understanding the impact of climate change on wildfire risk (Abatzoglou et al. 2019; Touma et al. 2021, 2022, 2023; Jain et al. 2022). We use a modified version of the FWI to quantify

fire weather conditions in the simulations to overcome the lack of sub-daily data availability. The FWI is calculated for the CESM2-LE using surface daily precipitation (CESM2 variable name: PRECT, abbreviation: *pr*), maximum temperature (TREFHTMX, *tasmax*), relative humidity (RHREFHT, *hurs*), and surface windspeed (U10, *sfcWind*). We first calculate the three moisture codes that reflect conditions for three depths of fuel and time scales. Each moisture code has a fuel drying and wetting (or rainfall) phase that are calculated sequentially. The Fine Fuel Moisture Code (FFMC) reflects moisture levels for shaded litter fuels and on daily time scales and is calculated using *tasmax*, *hurs*, and *sfcWind* for fuel drying, and *pr* for fuel wetting. The Duff Moisture Code (DMC) reflects moisture levels for decomposed organic material and on monthly timescales and is calculated using *pr* for fuel wetting, and *tasmax* and *hurs* for fuel drying. The Drought Code (DC) reflects moisture levels for deep litter and soil and is computed using *pr* for the rainfall phase and *tasmax* for the drying phase. Using the FFMC and *sfcWind*, the Initial Spread Index (ISI) is then calculated to represent the fire spread rate, and using the DMC and DC, the Build-Up Index (BUI) is calculated to represent the potential heat release and severity of fire. Lastly, the ISI and BUI are used to calculate the FWI and represents overall fire danger. All moisture codes and indices are unitless.

We compare the FWI calculated from the CESM2-LE for JJASO to those calculated from observationally-based gridMET variables (Abatzoglou 2013) over the western U.S. from 1983-2024. We show that the mean FWI is generally biased low in CESM2-LE compared to the mean gridMET FWI, and that the 99<sup>th</sup> percentile of the FWI is biased high (Supplementary Figure 1). While the CESM2-LE captures some large-scale spatial variations in FWI mean and extreme values (e.g., over the Rocky Mountains), smaller-scale variations are not reflected, such as over the Sierra Nevada or the Cascade mountain ranges. The bias in the mean FWI is similar to that found in Gallo et al. (2023), who calculated FWI for 16 CMIP6 models (excluding CESM2) and found that the multimodel mean of FWI was biased low for the western U.S. We note that the biases are largely systematic over the region, giving us more confidence in using model-based thresholds and analyzing time periods in model data only (i.e., we do not compare future projections with observations).

### *c. Extreme event definition and baselines*

To identify extreme fire weather events, we use the location-specific 99<sup>th</sup> percentile of the FWI across the full 100-member ensemble. Previous studies shown that 95<sup>th</sup> percentile and

above of FWI is well-correlated with large and severe wildfires in the western U.S. (Goss et al. 2020; Jain et al. 2024). While we do not employ a sensitivity analysis to explore the robustness of our results to the 99<sup>th</sup> percentile threshold, previous studies have shown that using a lower threshold (e.g., 95<sup>th</sup> percentile) results in similar relative spatial patterns of extreme fire weather events, with more frequent events but smaller relative increases in future periods (Touma et al. 2022) and earlier emergence of future extreme fire weather frequency above the historic variability (Abatzoglou et al. 2019). We use the full ensemble to calculate the 99<sup>th</sup> percentile to robustly account for internal climate variability when estimating extreme values. We use two baseline types to calculate the 99<sup>th</sup> percentile threshold and associated FWI variable (*pr*, *tasmax*, *hurs*, and *sfcWind*) anomalies: (1) a “fixed” baseline 35-year period centered around 1980, and (2) a “moving” baseline 35-year period centered around each year in the timeseries. We use all calendar day values of the FWI to calculate the percentile threshold value. Using a 35-year period allows us to capture interannual to decadal variability of the FWI and reduce the sensitivity to the exact set of years used to define the baseline. The threshold using the fixed baseline is constant in time, while that with the moving baseline changes from year-to-year. By using a moving baseline, we can begin to isolate the long-term, thermodynamically driven trends in the characteristics of extreme fire weather events from the short-term variations of these characteristics. These two approaches bookend the range of potential adaptation to long term changes – the fixed threshold assumes no adaptation while the moving threshold assumes continued adaptation to the mean climate. Figure 1 a and b shows an example of these thresholds and identified exceedances for a grid point near Los Angeles.

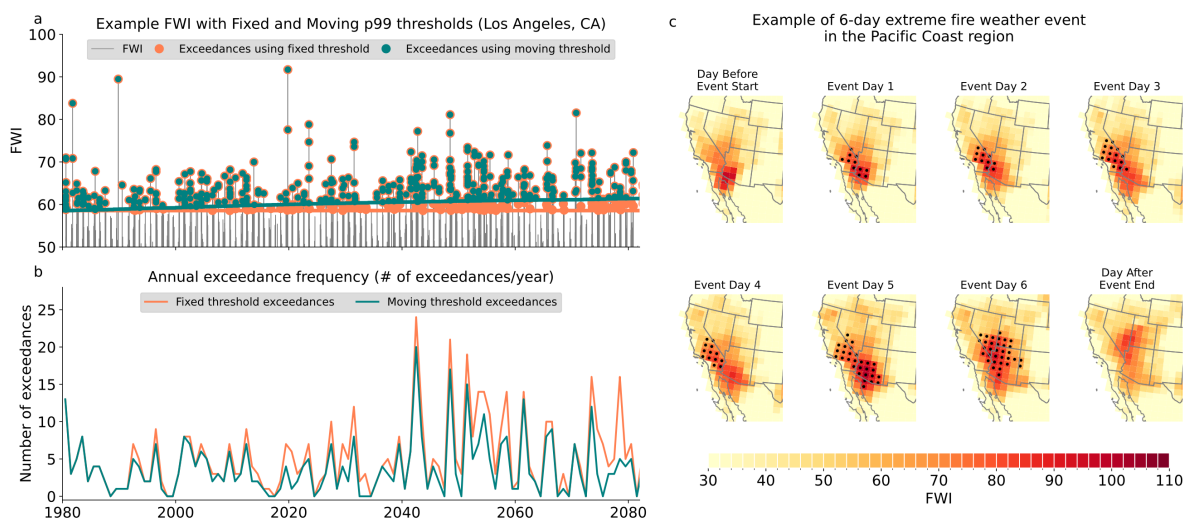




Fig. 1. a) Example FWI time series for one grid point near Los Angeles and one ensemble member (1001.001), with fixed and moving 99th percentile thresholds and identified exceedances. b) Annual number of exceedances calculated from (a) fixed and moving thresholds. c) Example of a 6-day extreme fire weather event over the Pacific Coast region. The shading represents the value of FWI, and the black dots represent the identified spatiotemporally connected event. The event starts when at least one grid point in the regional boundary of the Pacific Coast region (shown in Figure 3) exceeds the local threshold and the event ends when there are no longer any grid points that are spatiotemporally connected to that event within the region boundary.

#### d. Event identification

For each ensemble member and each threshold type, we identify grid points that meet or exceed the 99<sup>th</sup> percentile FWI threshold for each timestep. We use a framework with image processing functions from the *Scipy* Python package (Virtanen et al. 2020) to identify spatiotemporally connected grid points that exceed the extreme threshold. We first spatially subset the FWI dataset from 0-90°N and 0-180°W to increase computational efficiency but ensure that events are not truncated spuriously. We then create a binary dataset, where grid points that meet or exceed the extreme threshold are equal to 1, and those that fall below the threshold are equal to 0. We then identify spatiotemporally connected grid points that are equal to 1 – for spatial connectivity, grid points must be connected by their edges or vertices and for temporal connectivity, at least one grid point within the event must be equal to 1 on two continuous days. Events can be as small as one grid cell, and as short as one day. We identify events continuously for the full analysis period for all calendar days. The duration and cumulative area of each event is calculated, as well as the corresponding FWI values and FWI input variable anomalies throughout the event.

We identify events for eight U.S. regions (7 individual states, with California separated into northern and southern portions along 37N) and two regional groupings that have historically experienced large and severe wildfires. These are as follows: Pacific Coast group, comprised of Southern and Northern California, Oregon and Washington; Four Corners group, comprised of New Mexico, Arizona, Utah and Colorado. We then find events that have at least one grid point within the bounds of a region or region group of interest for the full duration of the event. If an event in the full event dataset “leaves” the region or region group and then “returns”, it is considered two distinct events. For region groups, we subset the dataset for the full region group simultaneously. This ensures that we do not double count events when events span multiple regions within the group simultaneously. We show an example of a 6-day event that occurred in the Pacific Coast region in Figure 1c.

#### e. Event analysis

For each event, we calculate its total duration (number of event days), area within the region and intensity (event-maximum FWI). We also calculate the anomalies of *pr*, *tasmax*, *hurs*, and *sfcWind* during the event using the 30-day, 35-year fixed baseline (1963-1997) mean for events identified using a fixed threshold and using the 30-day, 35-year moving baseline mean for those identified using a moving threshold. The 30-day moving mean allows us to account for the seasonal patterns of the FWI input variables. We specify which type of baseline is being used when describing any relevant results.

We create annual distributions of event characteristics including event frequency, number of events days, area and intensity, as well as for the FWI input variables, for each season and region by first averaging over all events in each ensemble member in each season and region and then grouping those averages together to create a distribution (100 values representing an ensemble member each). We summarize these time-evolving distributions using the 25<sup>th</sup>, 50<sup>th</sup>, and 75<sup>th</sup> percentiles, or the interquartile range (IQR).

We also create composites for each period and each ensemble member for grid point- and event-specific values of the number of events, annual number of event days, area, and intensity, as well as *pr*, *tasmax*, *hurs*, and *sfcWind* anomalies. We also show vapor pressure and vapor pressure deficit (VPD) anomalies to decouple temperature changes from those in relative humidity. Because vapor pressure and VPD are not available CESM2-LE output variables, we calculate saturation vapor pressure ( $e_s$ ):

$$e_s = 6.11 \times 10^{\left(\frac{7.5 \times tas}{237.3 + tas}\right)} \quad (\text{Equation 1})$$

where *tas* is the near surface air temperature in °C and  $e_s$  is in hPa. We then calculate actual vapor pressure ( $e$ ):

$$e = e_s \times hurs / 100 \quad (\text{Equation 2})$$

where  $e$  is also in hPa. We then calculate VPD as the difference between  $e_s$  and  $e$ .

#### f. Period definitions

We use three time periods to summarize extreme fire weather event characteristics over time. These are a historic period (1980-2014), an early future period (2015-2050), and a late future period (2051-2082). We end the last period in 2082 because we use 35-year moving windows to calculate the moving thresholds and means. We calculate changes in the

characteristics of fire weather events for the two future periods relative to the historic period. Additionally, we show time series of extreme fire weather event characteristics for the eight regions, with changes computed from the historic period.

*g. Isolating the impact of changes in the mean and variability of FWI variables*

We isolate the effect of changes in *pr*, *tasmax*, *hurs*, and *sfcWind* on the characteristics of extreme fire weather events. We create new “mapped” (*m*) time series for each variable and ensemble member (*n*) ( $pr_m^n$ ,  $tasmax_m^n$ ,  $hurs_m^n$ , and  $sfcWind_m^n$ ) using quantile mapping in order to restrict the whole time series to the 100-member monthly distribution in the fixed reference period using the following steps (see Figure 2 and Supplementary Figure 2). For each day of the time series, we first find the percentile of the value of the variable within its 100-member, 30-day, 35-year moving window distribution. We then find the corresponding value of that percentile in the 30-day, 35-year, 100-member distribution of the fixed baseline period centered around 1980 (Figure 2). By mapping the FWI variable time series to the fixed period, we maintain the relative day-to-day variability and spatial patterns between the mapped variable and the other unmapped variables but ensure that the variability and mean of the timeseries is constrained to that of the historic distribution. We then calculate four “mapped” FWI time series for each ensemble member using one of the newly mapped variables and keeping the other variables at their original values (*o*) (*e.g.*,  $FWI_{pr,m}^n = f(pr_m^n, tasmax_o^n, hurs_o^n, sfcWind_o^n)$ ). Using these four mapped FWI timeseries for each ensemble member, we identify and quantify the characteristics of extreme fire weather events as previously described. These events and their characteristics are considered to represent events in which one of the variables is not impacted by forced changes in the mean *and* variability. We then compare the event characteristics using the mapped and original FWI time series to assess the contribution of changes in the full distribution (*i.e.*, mean and variability) of each variable to changes in extreme fire weather events.

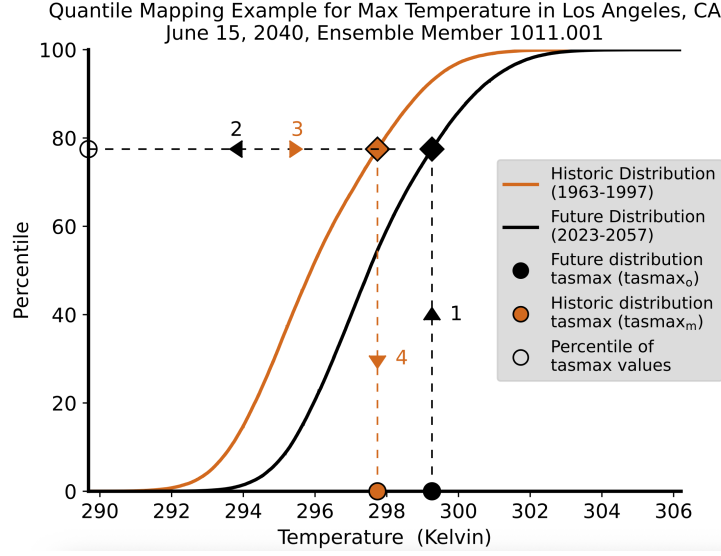


Fig. 2: Schematic of quantile mapping for maximum temperature for June 15, 2040 for a grid point near Los Angeles, CA for ensemble number 1011.001 using its 100-member future distribution (June 1-30, 2023-2057) and the 100-member historic (June 1-30, 1963-1997) distribution. The historic period is captured using a 35-year period centered around 1980, while the future distribution is captured using a 35-year period centered around 2040. The black line and markers represent the future distribution and values, respectively, and the orange lines and markers represent the historic distribution and values, respectively. Steps 1&2: Using the  $tasmax_o$  value from the future distribution, find the percentile value; steps 3&4: Using that percentile value find the  $tasmax_m$  from the historic distribution.

We also create new time series with only forced changes in the mean removed for each variable (see Supplementary Figure 2). By comparing to the original time series, we isolate the impact of forced changes in the mean of each variable on extreme fire weather event characteristics. For each variable, we calculate forced changes in the mean using the difference between the moving 30-day, 35-year, 100-member mean and the fixed (1980) 30-day, 35-year, 100-member mean. We then remove these forced changes in the mean from each respective time series for each ensemble member to create four new “detrended” ( $d$ ) time series ( $pr_d^n, tasmax_d^n, hurs_d^n, and sfcWind_d^n$ ). As before, we use these new time series to calculate the FWI four additional times, each time using one of the new timeseries with the mean removed for one of the variables, while all other variables use their original time series (e.g.,  $FWI_{pr,d}^n = f(pr_d^n, tasmax_o^n, hurs_o^n, sfcWind_o^n)$ ). Using these four new FWI timeseries for each ensemble member, we identify and quantify the characteristics of extreme fire weather events as previously described. These events and their characteristics are considered to represent events in which one of the variables is not impacted by forced changes in the mean. The difference between the quantile mapped and the detrended extreme

fire weather events is used to estimate the effect of changes in the variability on the seasonal average of that variable (see Supplementary Figure 2).

### 3. Results

#### *a. Historic characteristics of extreme fire weather events*

Figure 3 shows composite maps of the number of extreme fire weather event days per year for the Pacific Coast and Four Corners regions using fixed and moving thresholds for June to October (JJASO) – the height of the wildfire season in the western U.S. During the historic period, the fixed baseline shows similar patterns to the moving baseline though with smaller magnitudes because the time period used for the fixed threshold is slightly earlier than the moving threshold centers used in the composite maps (1963-1997 vs 1980-2014) (Figure 3 a, d, g, and j). We find that events that are partially or fully located in the Pacific Coast region tend to occur more frequently on the eastern edge of the region (>10 event days/year) relative to coastal areas (~8 event days/year), and tend to extend further eastwards into Montana, Idaho, Nevada and Arizona (~5 event days/year), southward into Baja California and northward into western Canada (Figure 3 a and g). Four Corners events largely occur in Arizona and Utah (>12 event days/year), with fewer event days occurring in Colorado and New Mexico, especially across the Rocky Mountains. Similarly, extreme fire weather events spread towards the north, reaching Idaho and Wyoming, and towards the west, reaching into Nevada and California (Figure 3 d and j). We note that, because the thresholds are based on 35-year periods centered on either the fixed threshold year or the moving threshold year and using the full 100-member ensemble, there is some variability in terms of the expected exceedances, with number of event days being higher than the expected 1% of days per year (3.65 days/year).

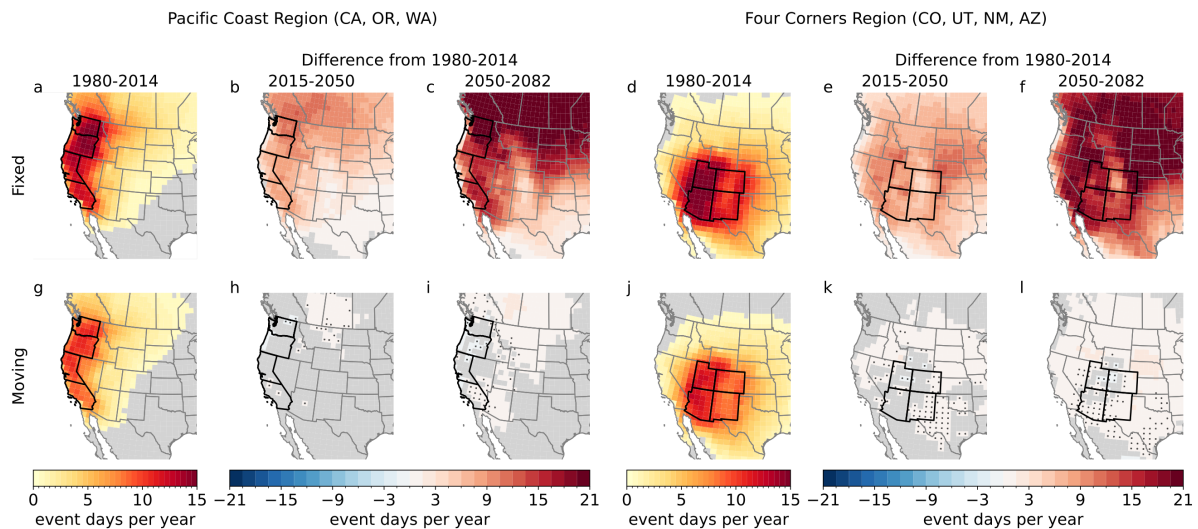


Fig. 3. Total number of event days per year over each grid point in the (a, d, g, and j) historic period (1980-2014) and change in the number of event days per year over each grid point in future periods (b, c, e, f, h, i, k, and l) using fixed (a-f) and moving (g-l) threshold for events fully or partially located in the Pacific Coast (a-c and g-f) and in the Four Corners (d-f, j-l) regions in JJASO. For the historic period, all shaded locations have at least 0.66 event days/year, meaning that at least two-thirds of the ensembles show one event day/year on average. Similarly, for the future period changes, all shaded locations have an increase or decrease of at least 0.33 event days/year. Stippling indicates that the difference from the historic period is not statistically significant ( $p\text{-value} \leq 0.05$ ).

### *b. Projected changes in extreme fire weather event characteristics*

Extreme fire weather events become more frequent, last longer, and cover larger areas by the end of the 21st century when using the fixed threshold compared to the moving threshold (Figures 3 and 4). In the Pacific Coast, events tend to become more frequent in the eastern parts of the region and more widespread towards the north and east, with up to an additional ~15 event days/year reaching the Midwest, and an additional ~21 event days/year reaching western Canada in the late future period (Figure 3 c). The largest increases occur in Washington, with approximately two more events/year, which also last two more days on average and cover 20,000 km<sup>2</sup> more in the late future compared to the historic period (Figure 4 d, h, and l). In the southern part of the region, increases in event duration and area are still significant but are slightly reduced in magnitude, with the smallest increases occurring in Southern California (Figure 4 e and i). Events tend to become more connected and extend in all cardinal directions in the Four Corners region in the future compared to the historic period, with the largest spread towards southern Idaho and Nebraska (>15 more event days/year; Figure 3 e and f). Here, we find that extreme fire weather event duration and area increase similarly across all four states – events are approximately two days longer and cover

approximately 10,000 km<sup>2</sup> more than in the historic period (Figure 4 q-x). Interestingly, increases in event area and extent are constrained by the Southern Rocky Mountain Range, but not by the Middle or Northern/Canadian Rocky Mountain Ranges for both the Pacific Coast and Four Corners regions (Figure 3).

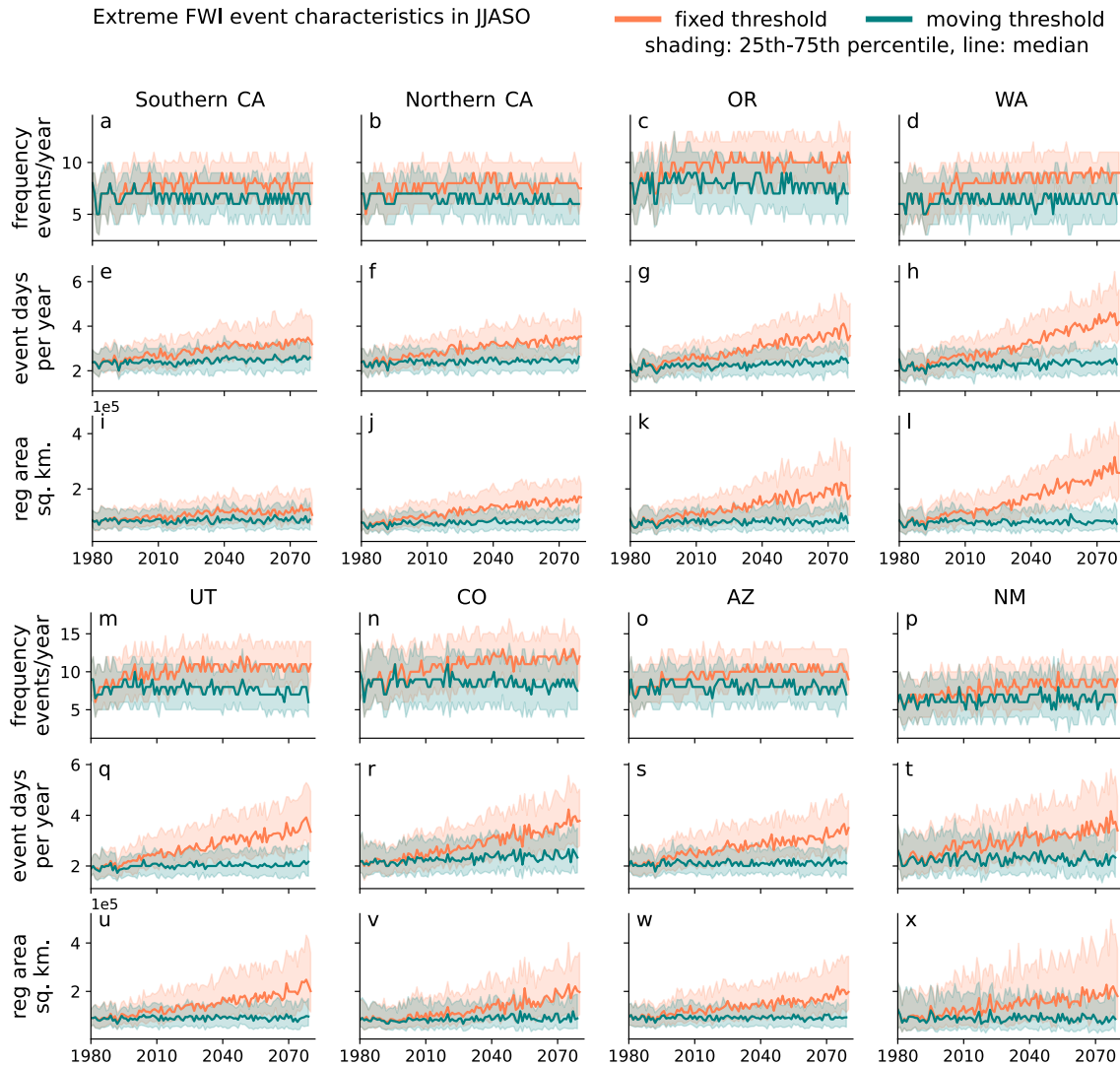


Fig. 4. Frequency (a-d and m-p), duration (e-h and q-t), and state-bound area (i-l and u-y) of extreme fire weather events using a fixed (coral) and moving (teal) 99<sup>th</sup> percentile threshold for events in the Pacific Coast (a-l) and Four Corners (m-y) regions for JJASO.

While the annual frequency of event days for each location using the moving threshold is explicitly set by the threshold (1% of days), the duration and spatial connectivity of the events is not explicitly bounded. Specifically, these 1% of event days could occur more closely together in both space and time due to changes in the spatial or temporal variability of the FWI and therefore could change the area and duration of events. We see evidence of small but robust increases in the number of event days, generally occurring to the north and

east of the Pacific Coast region and to the northeast and northwest of the Four Corners region (Figure 3 h and i). While these changes seem small and negligible compared to a fixed threshold, they point to changes in areas and durations of events that are not reflected in the thermodynamic shift of the FWI distribution and instead point to the effects of changes in the FWI distribution that may be non-thermodynamic. Specifically, the spread of events beyond the specified region shown when using the moving baseline are likely driven by dynamic processes.

*c. Meteorological conditions underlying future changes in extreme fire weather events*

In the Pacific Coast region, extreme fire weather events in the historical period are characterized by positive anomalies in maximum temperature (up to 10 degrees K) and wind speed (up to 2 m/s), and negative anomalies in relative humidity (up to -25%) and precipitation (up to -2 mm/day) compared to the historical 1963-1997 30-day mean (see Methods; Figure 5 a, d, g, j, n, p, s and v). In the late future period, extreme fire weather events identified using a fixed threshold show an increase in maximum temperature anomalies by up to 4 degrees Kelvin throughout the Pacific Coast region compared to the historic period (Figures 5 i and 6 e-h). Changes in other FWI input variables are more spatially heterogeneous: precipitation anomalies tend to become less negative over California and more negative over Oregon and Washington; relative humidity anomalies tend to become less negative over the coast (+4%) and more negative over the interior of the region (-4%); and windspeeds tend to be about 0.5 m/s slower over the northern half of the region but unchanging in the southern part of the region (Figures 5 b, c, n, o, t, and u, and 6 a-d and i-p). The changes in these input variables during extreme fire weather events are more acute than when considering all days in JJASO (Supplementary Figure 3). We also note that, while not included in the calculation of the FWI, actual vapor pressure anomalies increase along with vapor pressure deficit (VPD) anomalies, reflecting similar changes in relative humidity inland, but opposite changes on the coast (Supplementary Figure 4).

For the moving threshold case, we employed a moving 35-year mean of the FWI input variables from which to calculate the anomalies (see Methods) to allow for consistency in the context of the threshold that is used to define the events. For these events, future increases in temperature anomalies during extreme fire weather events are limited to < 1 K (Figures 5 k and l, and 6 e-h). This means that for events to occur (i.e., for the FWI to exceed the 99th percentile threshold) maximum temperature anomalies compared to the contemporaneous 35-



year mean are only slightly warmer. However, precipitation anomalies fall further below the mean throughout the Pacific Coast region in the future periods (up to 10% lower in some locations), with larger decreases occurring in the eastern part of the region (Figures 5 e and f, and 6 a-d). Some of these larger negative anomalies are occurring where mean precipitation is increasing in future climates (Supplementary Figure 3), causing extreme fire weather events to be relatively much drier than the moving mean. Events on the coast are also becoming more humid, while interior events become less humid, compared to the moving mean and events in the north are less windy, while events in the south see small but robust increases in windspeed compared to the moving mean (Figures 5 w and x, and 6 i-p).

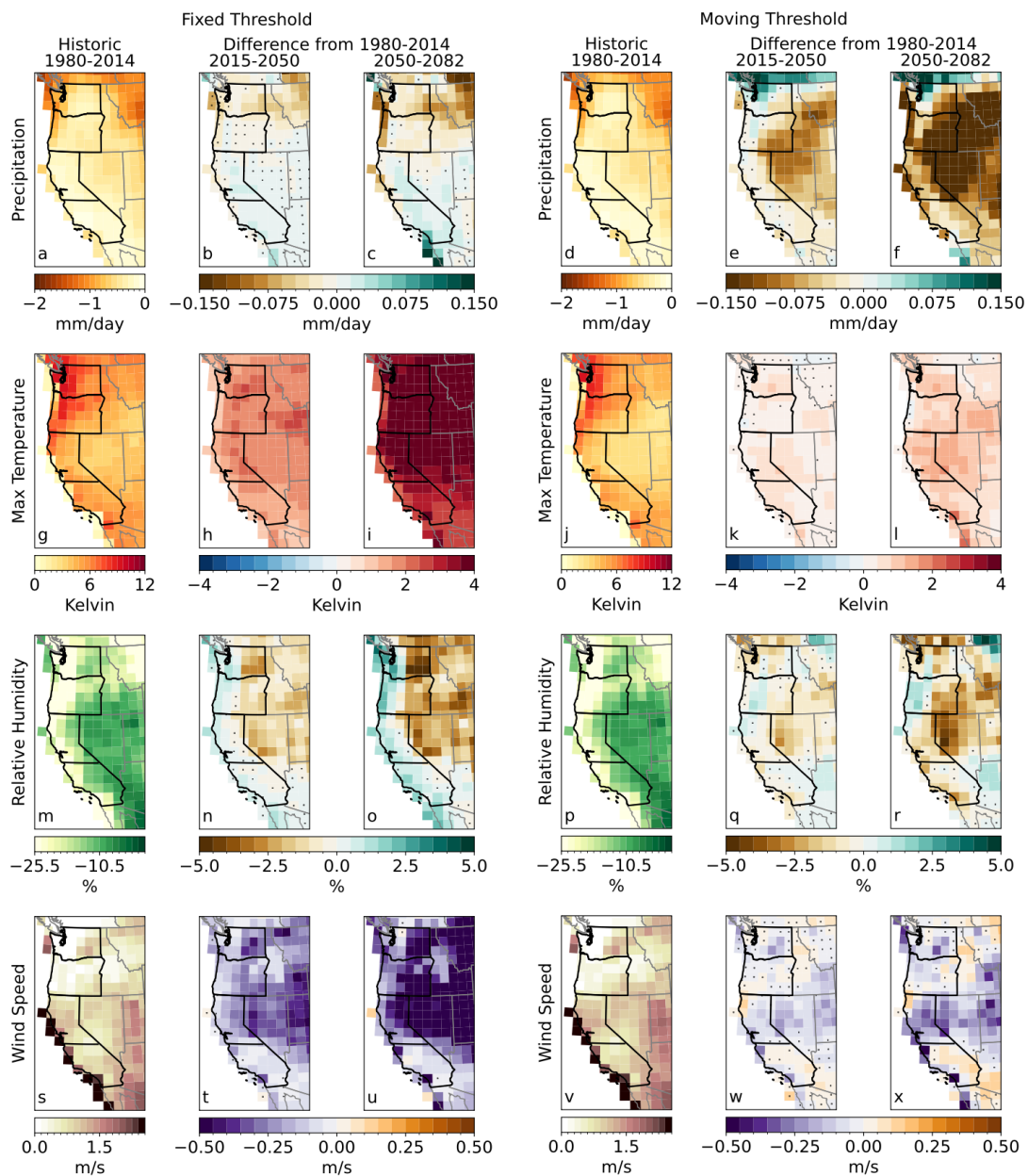


Fig. 5. (a, d, g, j, m, p, s, v) Composite maps of precipitation (mm/day), maximum temperature (Kelvin), relative humidity (%), and wind speed (m/s) anomalies during extreme fire weather events using (a, g, m, s) 30-day, 35-year fixed mean for the fixed threshold events, and (d, j, p, v) 30-day, 35-year moving mean for the moving threshold events in the Pacific Coast region in JJASO for the historic period (1980-2014). (b, c, e, f, h, I, k, l, n, o, q, r, t, u, w, x) composite maps showing the changes in these fire weather variables in the two future periods for the fixed and moving thresholds for 2015-2050 and 2050-2082. The composites are created by averaging the variable anomalies over the area and duration of all events across all ensemble members in each period. Stippling indicates that the difference from the historic period is not statistically significant ( $p\text{-value} \leq 0.05$ ).

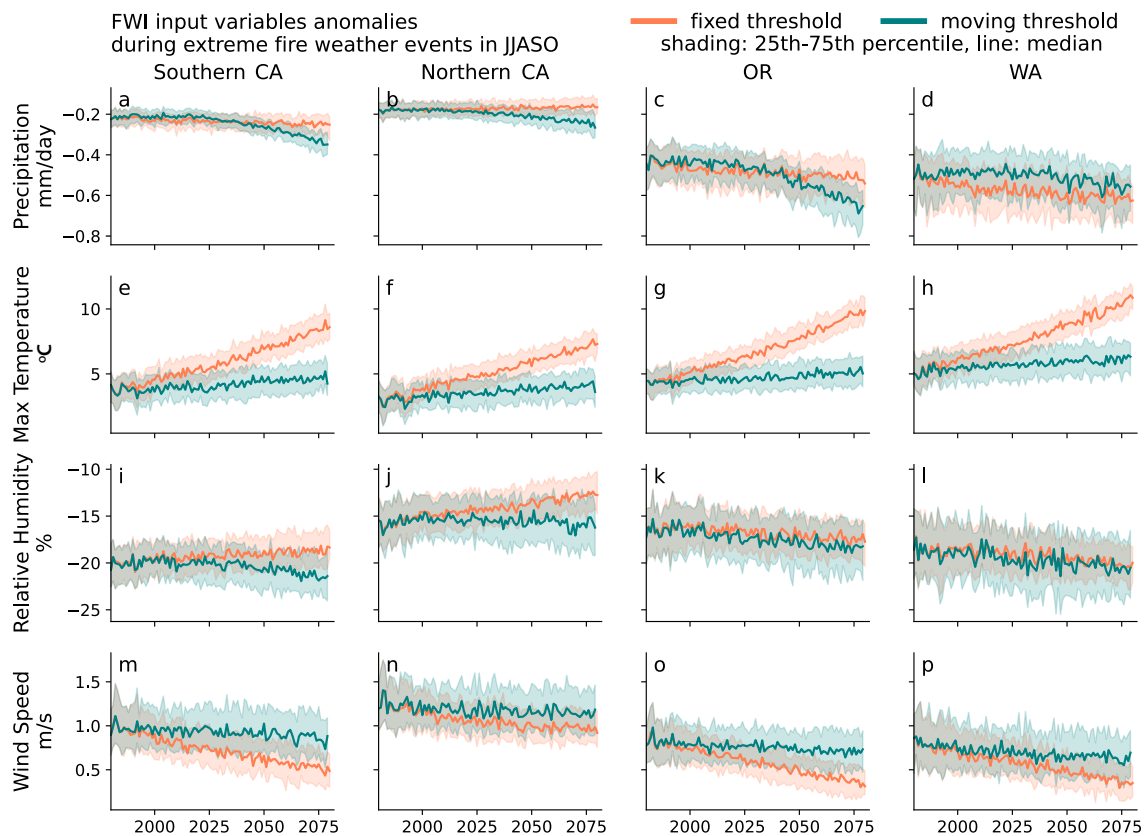


Fig. 6. Time series of precipitation (a-d), maximum temperature (e-h), relative humidity (i-l) and wind speed (m-p) anomalies during extreme fire weather events in JJASO in Southern California (CA; a, e, i, m), Northern CA (b, f, j, n), Oregon (OR; c, g, k, o) and Washington (WA; d, h, l, p) using the fixed mean and threshold (coral) and the moving mean and threshold (teal).

Events identified using a fixed threshold in the Four Corners region also show large future increases in maximum temperature of up to 4 K (Figure 7 c). The largest increases in maximum temperature occur in Utah and Colorado, coinciding with decreases in relative humidity and increases in windspeed (Figures 7 c, e, g and 8 e, f, i, j, m, n). Events in the Rocky Mountains have the largest negative anomalies in precipitation and relative humidity

in the historic period, and these variables continue to decrease in the future periods by 0.15 mm/day and 2%, respectively – however, this area shows relatively few event days/year in the historic period as well as smaller increases in the number of event days/year compared to other regions (Figures 3 d-f, and 7 a and e). Therefore, while these events are becoming drier, lower precipitation and relative humidity are not necessarily driving increases in extreme fire weather events over this region. We also note that actual vapor pressure and VPD anomalies increase throughout the whole region during extreme fire weather events, which is reflected in changes in relative humidity in Colorado and Utah, but oppose the relative humidity trends in New Mexico and Arizona (Supplementary Figure 5). As in the Pacific Coast, events are generally less windy, with about 0.5 m/s decreases in windspeed over Utah and Colorado (Figures 7g and 8 m, n). Patterns similar to those in the Pacific Coast region also emerge for events identified using a moving threshold in the Four Corners region. Events are much drier, especially in the center of the region where mean precipitation is increasing (Supplementary Figure 3), and Utah and western Colorado show large decreases in relative humidity (Figures 7f and 8 i, j). Events have greater wind speeds in New Mexico and Arizona, but lower wind speeds in the northern part of the Four Corners region (Figures 7h and 8 m-p). Additionally, increases in maximum temperature are small and not significant for many parts of the region (Figures 7d and 8 a-d).

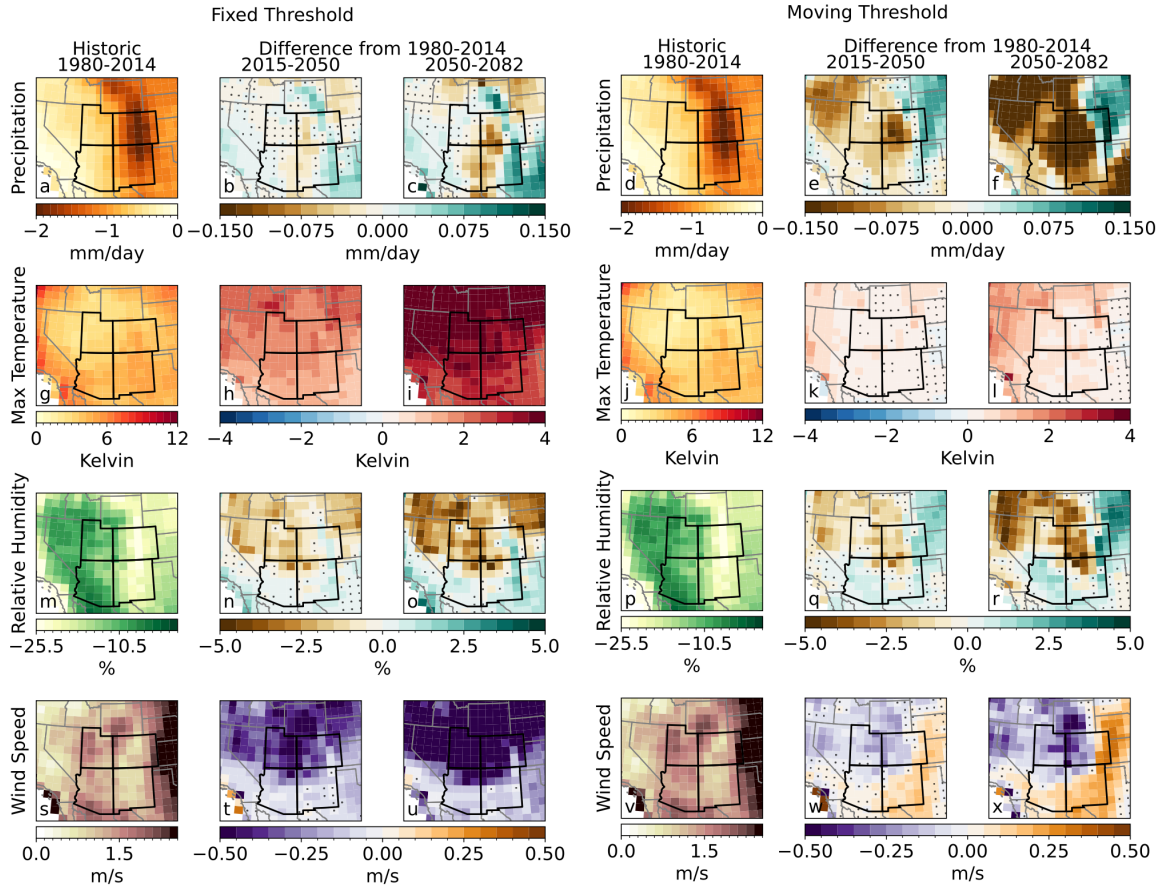


Fig. 7. (a, d, g, j, m, p, s, v) Composite maps of precipitation (mm/day), maximum temperature (Kelvin), relative humidity (%), and wind speed (m/s) anomalies during extreme fire weather events using (a, g, m, s) 30-day, 35-year fixed mean for the fixed threshold events, and (d, j, p, v) 30-day, 35-year moving mean for the moving threshold events in the Four Corners region in JJASO for the historic period (1980-2014). (b, c, e, f, h, i, k, l, n, o, q, r, t, u, w, x) composite maps showing the changes in these fire weather variables in the two future periods for the fixed and moving thresholds for 2015-2050 and 2050-2082. The composites are created by averaging the variable anomalies over the area and duration of all events across all ensemble members in each period. Stippling indicates that the difference from the historic period is not statistically significant ( $p\text{-value} \leq 0.05$ ).

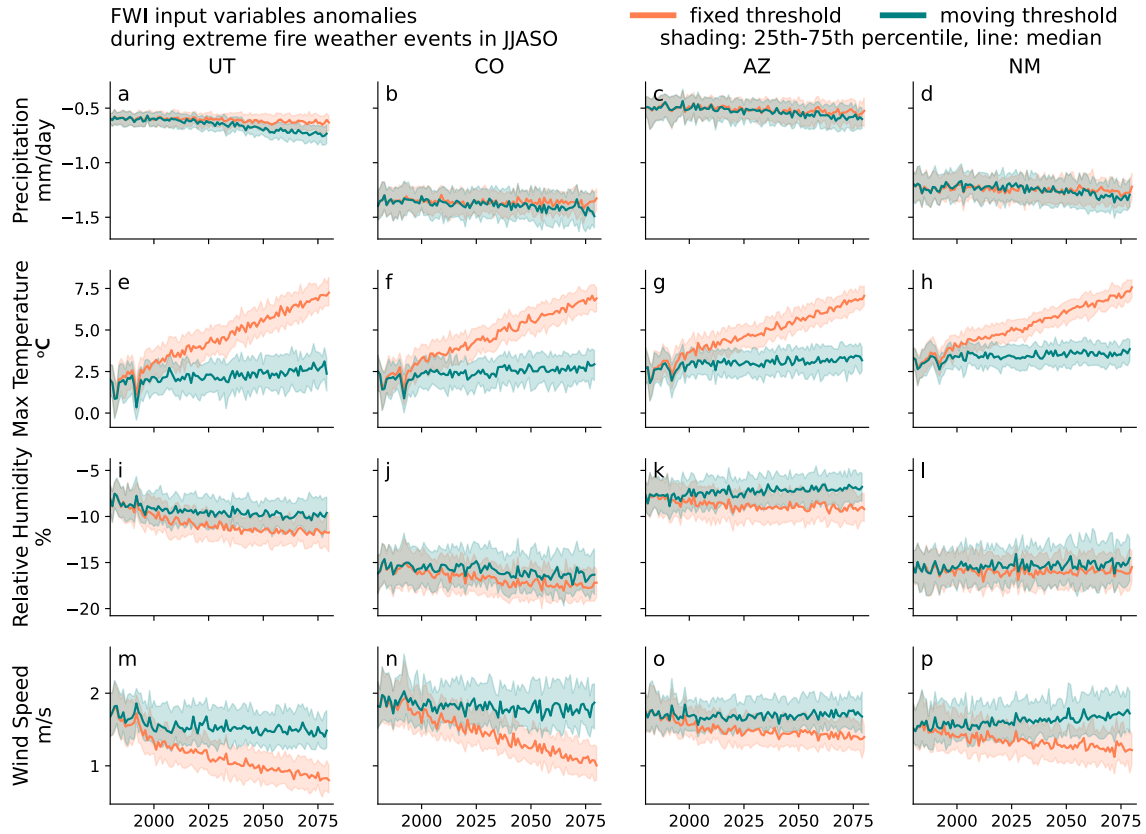


Fig. 8. Time series of precipitation (a-d), maximum temperature (e-h), relative humidity (i-l) and wind speed (m-p) anomalies during extreme fire weather events in JJASO in Utah (UT; a, e, i, m), Colorado (CO; b, f, j, n), Arizona (AZ; c, g, k, o) and New Mexico (NM; d, h, l, p) using the fixed mean and threshold (coral) and the moving mean and threshold (teal).

#### *d. Isolating the impact of individual fire weather variables*

While the previous results show how the underlying conditions of extreme fire weather events are projected to change, it is still unclear how changes in the mean and variability of each FWI input variable impact event characteristics. To investigate this, we use quantile and mean mapping approaches (see Methods, Figure 2 and Supplementary Figure 2) to isolate the impact of total changes, as well as changes in the mean and variability of maximum temperature, precipitation, relative humidity, and wind speed on the frequency, duration, area, and intensity of extreme fire weather events (identified using the fixed threshold) in the future periods for the Pacific Coast and Four Corners regions.

In the Pacific Coast region, mean increases in maximum temperature lead to the largest increases in extreme fire weather event frequency (up to ~1 event/year in some locations), number of event days (~10), area (~10,000,000 km<sup>2</sup>) and maximum intensity (~3 FWI units) in the late future period, while changes in the variability of maximum temperature have

minimal impacts on these event characteristics (Figure 9 e and f and Supplementary Figure 6). For all events in the Pacific Coast, mean increases in temperature lead to the largest increases in number of events, number of events days, and area compared to any changes in other variables (Figures 9 e and 10 b-d and Supplementary Figures 3 and 6).

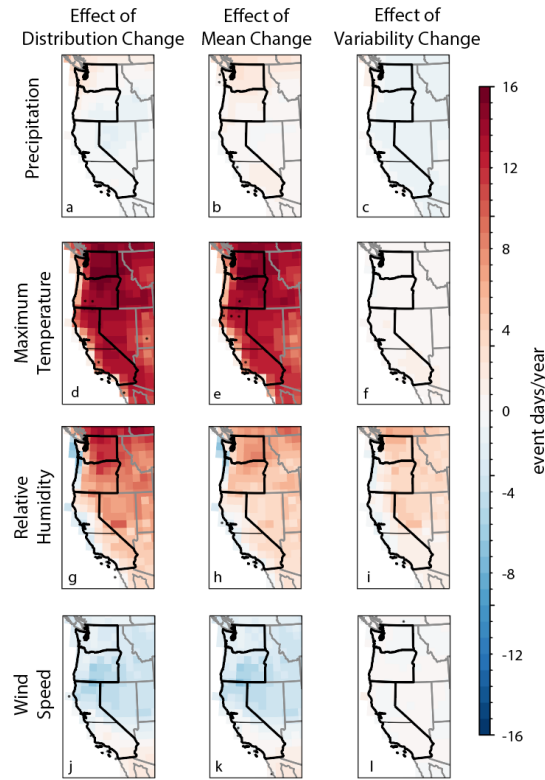


Fig. 9. The effect of changes in the distribution (a, d, g, j), mean (b, e, h, k) and variability (c, f, i, l) of precipitation (a-c), maximum temperature (d-f), relative humidity (g-i), and wind speed (j-l) on changes (from the historic period, 1980-2014) in the number of event days per year for the Pacific Coast region for JJASO in the late future period (2050-2082). These composites are created by averaging event characteristics for all events for each ensemble member for each period at each grid point. Then, the grid point-specific values of the historic period are subtracted from the late future period for each ensemble member, and the difference values are averaged over all ensemble members. Stippling indicates that the difference from the historic impacts is not significantly different ( $p < 0.05$ ). Results for event frequency, area, and intensity can be found in Supplementary Figure 6.



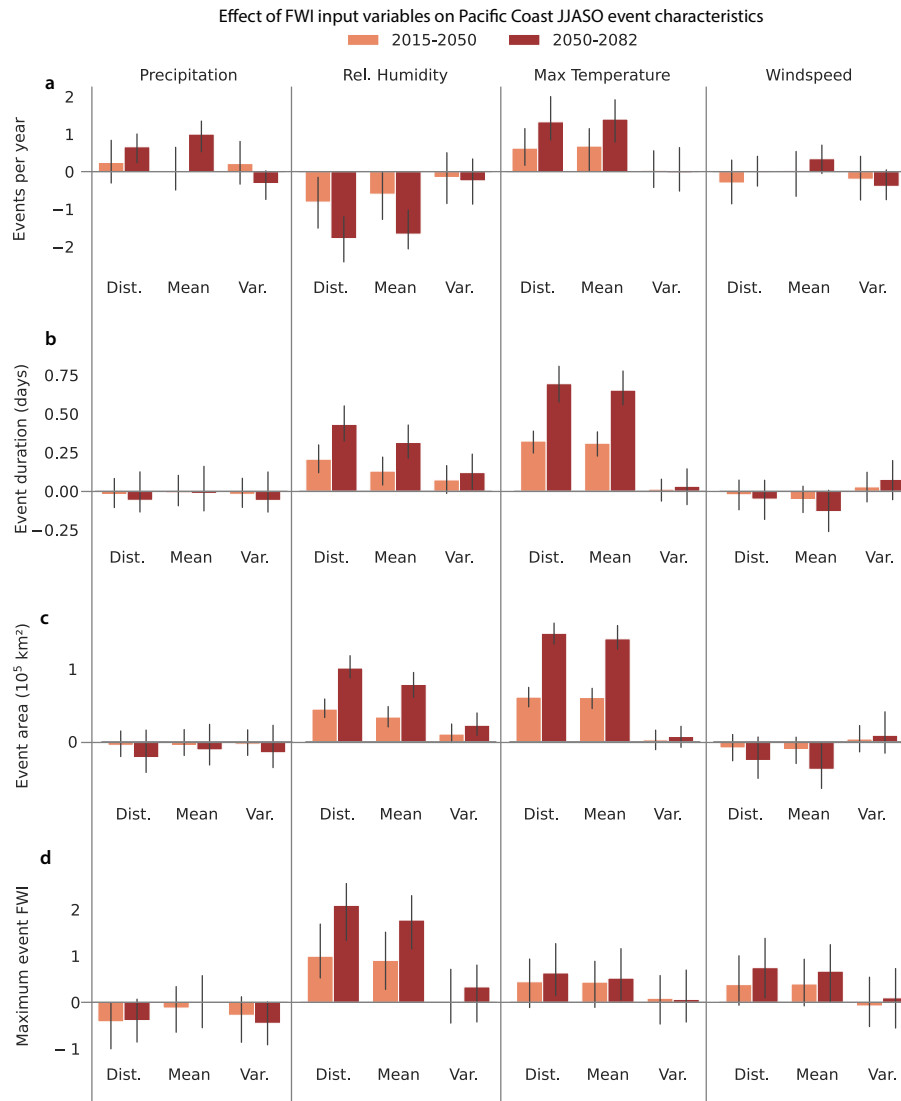


Fig. 10. The difference (from the historic period, 1980-2014) in the impact of changes in the full distribution (Dist.), mean, and variability (Diff.) of precipitation, relative humidity, maximum temperature and wind speed on (a) events per year, (b) events days per year, (c) regional event area, and (d) maximum regional event intensity FWI using the fixed threshold for the early (2015-2050, coral) and late future periods (2050-2082, red) for the Pacific Coast region in JJASO. The mean across all events for each ensemble member is first calculated, and we show the median across all ensemble members. The error bar represents 25<sup>th</sup> to the 75<sup>th</sup> percentile of the ensemble spread.

Compared to changes in mean maximum temperature, changes in mean relative humidity cause slightly smaller increases in the number of event days and area of extreme fire weather events in the late future period over the Pacific Coast region (Figures 9 h and 10 b and c and Supplementary Figure 6). While changes in mean relative humidity do lead to increases in the number of events and maximum FWI intensity in eastern Oregon and Washington, they also lead to decreases in the coastal areas and in much of California (up to -0.8 events/year and -4 FWI units in maximum FWI; Supplementary Figure 6). Unlike for

maximum temperature, we find that the changes in variability (obtained as the difference between the effects of changes in distribution and mean; see Methods and Supplementary Figure 2) of relative humidity also lead to substantial and significant changes in event characteristics in much of the Pacific Coast, and tend to amplify the total impact of relative humidity changes on extreme fire weather events (Figure 9 i and 10, and Supplementary Figure 6). This is especially evident for event duration and area, where changes in the mean and variability of relative humidity lead to increases of 0.25 and 0.1 event days/year and 80,000 and 20,000 km<sup>2</sup> in average event area, respectively, in the late future period (Figure 10 b and c). We note that changes in mean relative humidity leads to a spatially averaged reduction in number of events per year (Figure 10 a). These spatially averaged decreases are driven by large decreases on the WA coast and broad areas of decreases in California (Supplementary Figure 6). However, when considering the role of all variables combined, these decreases are opposed by larger increases due to changes in precipitation, maximum temperature and wind speed, especially in southern CA and WA (Supplementary Figure 6). The change in the mean of wind speed generally drives small decreases in event duration and area over the region but causes increases in the event frequency and maximum intensity of events in southern California (Figure 10 and Supplementary Figure 6). We hypothesize that higher mean wind speeds in southern California are leading to higher values of FWI when extreme fire weather events do occur but may also lead to the attrition and separation of events (Supplementary Figure 3). The impact of the changes in the variability of wind speed on event characteristics are relatively small in the region except for the maximum intensity of events in northern California where there is an increase of about 2 FWI units (Figures 9 i and 10 and Supplementary Figure 6).

In the Four Corners regions, the impacts of changes in the mean and variability of the FWI variables are somewhat similar to those in the Pacific Coast region. Mean changes in maximum temperature and relative humidity lead to large increases in event days/year (up to 15 and 8 days/year, respectively) and area (up to 10,000,000 and 8,000,000 km<sup>2</sup>, respectively) in the late future period (Figure 11 e and h and Supplementary Figure 7). The impact of changes in the variability of maximum temperature is relatively small. However, changes in the variability of relative humidity lead to substantial and robust increases in event days/year and event area (Figure 11 i and Supplementary Figure 7) – approximately equal to the increases due to changes in the mean of relative humidity when looking across all events and ensemble members (Figure 12 b and c). Changes in the mean and variability of relative



humidity also lead to spatially-varied impacts on event intensity in the Four Corners region (Supplementary Figure 6). For example, in the center of the region, there are small and not statistically significant changes in maximum intensity due to changes in the mean of relative humidity, but large and significant increases (approximately 6 FWI units,  $p\text{-value} \leq 0.05$ ) due to changes in the variability. However, overall, changes in the mean of relative humidity lead to slight and non-robust increases in maximum event intensity, but changes in the variability lead to large decreases (-0.5 FWI units in the late future period; Figure 12 d). Like the Pacific Coast, changes in the mean of wind speed also lead to overall decreases in the number of event days/year (-4 event days/year) and event area (-4,000,000 km<sup>2</sup>), but are generally overwhelmed by the increases due to changes in other variables (Figure 11 k and Supplementary Figure 9). However, in western Colorado, the large decreases in event intensity due to mean changes in wind speed (up to -10 FWI units) are also reflected in the changes due to all variables (up to -2 FWI units; Supplementary Figure 7).

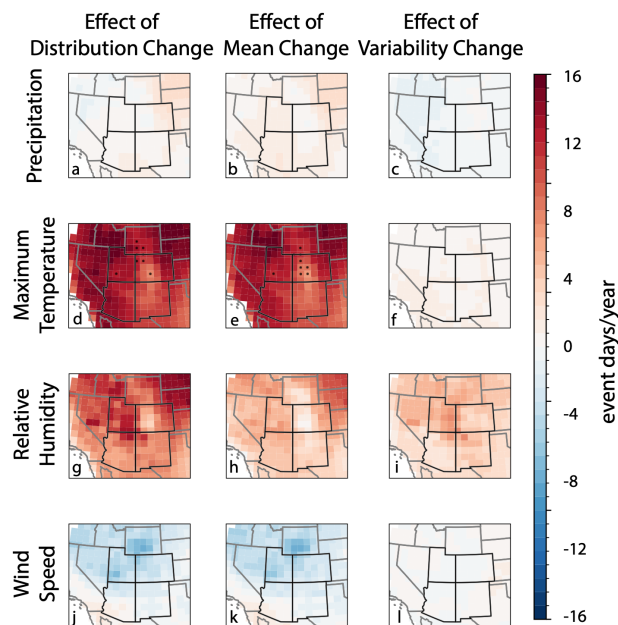
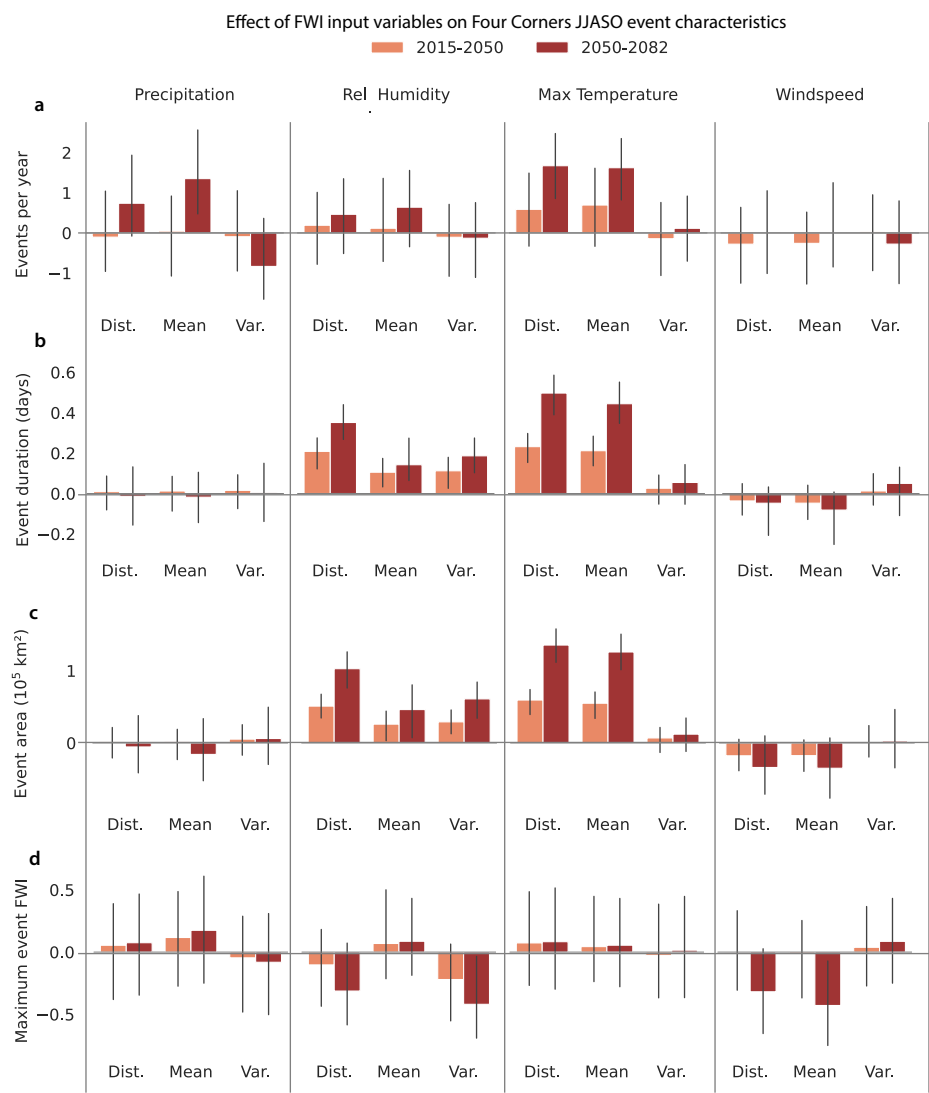


Fig. 11. The effect of changes in the distribution (a, d, g, j), mean (b, e, h, k) and variability c, f, i, l) of precipitation (a-c), maximum temperature (d-f), relative humidity (g-i), and wind speed (j-l) on changes (from the historic period, 1980-2014) in the number of event days per for the Four Corners region for JJASO in the late future period (2050-2082). These composites are created by averaging event characteristics for all events for each ensemble member for each period at each grid point. Then, the grid point-specific values of the historic period are subtracted from the late future period for each ensemble member, and the difference values are averaged over all ensemble members. Stippling indicates that the difference from the historic impacts is not significantly different ( $p < 0.05$ ). Results for event frequency, area, and intensity can be found in Supplementary Figure 7.



607 Fig. 12. The difference (from the historic period, 1980-2014) in the impact of changes  
608 in the full distribution (Dist.), mean, and variability (Var.) of precipitation, relative humidity,  
609 maximum temperature and wind speed on (a) events per year, (b) events days per year, (c)  
610 regional event area, and (d) maximum regional event intensity FWI using the fixed threshold  
611 for the early (2015-2050, coral) and late future periods (2050-2082, red) for the Four Corners  
612 region in JJASO. The mean across all events for each ensemble member is first calculated,  
613 and we show the median across all ensemble members. The error bar represents 25<sup>th</sup> to 75<sup>th</sup>  
614 percentile of the ensemble spread.

615 In both the Pacific Coast and Four Corners regions, changes in the mean of maximum  
616 temperature and in the mean and variability of relative humidity have the largest influences  
617 on extreme fire weather event frequency, duration, area and intensity. On the other hand, the  
618 impact of changes in wind speed are generally small, not significant, and varied, and changes

in precipitation also plays a relatively small role in the changes of extreme fire weather event characteristics for both early and late future periods.

## 4. Discussion

Our study employs the CESM2 Large Ensemble to investigate projections of extreme fire weather event characteristics for current and emerging fire-prone regions, specifically, the Pacific Coast and Four Corners regions. Using a fixed threshold, we find that the frequency, duration, and area of extreme fire weather events are projected to increase under a high-emissions scenario and projected to extend well-beyond regional boundaries. By the end of the 21<sup>st</sup> century, events in the Pacific Region are expected to reach north towards Canada and east towards the Midwest, and events in the Four Corners regions are expected to reach northeast towards the Midwest and west and northwest towards Idaho, Nevada, and southern California. These increases in extreme fire weather event duration, area, and intensity are fueled by increasing maximum temperature means, decreasing relative humidity means, as well as changes in the variability of relative humidity that are not reflected in the mean changes. When using a moving threshold, event frequency, duration, and area are generally unchanging in the future periods, but some expansion of spatiotemporally connected events towards similar regions as the fixed thresholds is evident, reflecting changes that are not explained by the long-term, mean climate trend. Additionally, extreme fire weather events using a moving threshold are only slightly warmer than the contemporaneous mean maximum temperature, but occur under much drier conditions, reflected in the underlying anomalously low precipitation and relative humidity. These changes may reflect the increases in mean precipitation throughout the future period that result in larger anomalies during extreme fire weather events.

We find that the choice of the baseline or threshold period used to investigate extreme fire weather events is highly important for making inferences about future events. In our case, we used two contrasting baselines: a fixed threshold that relies on the distribution of the FWI in the historical period only, and a moving threshold that accounts for an evolving FWI distribution. The relevance of a fixed *vs.* moving baseline for understanding the risk of extreme fire weather events in a particular region depends on the timescales at which communities and ecosystems adapt to changes in mean climate *vs.* climate variability. The moving threshold also allows insight into the drivers of future extreme fire weather events beyond the thermodynamically imposed shift in the FWI distribution. Similar considerations

apply to other types of extremes, for example marine (Deser et al. 2024; Amaya et al. 2023; Capotondi et al. 2024; Smith et al. 2025) and terrestrial heat waves (Skinner et al. 2025; Vogel et al. 2020). As far as we know, this is the first study to explicitly compare the impacts of projected changes in mean climate vs. climate variability on the characteristics of extreme fire weather events, and to quantify the underlying meteorological drivers of such changes.

By using a moving threshold, we can bring to light changes in event characteristics that may be due to changes in spatial or temporal variability of the FWI distribution that are not obvious when using a fixed threshold. In other words, we are able to isolate the changes in extreme fire weather events that are not due to the thermodynamically driven trends in the FWI and that may act on relatively shorter time scales. We find some changes in extreme fire weather event characteristics when using a moving threshold, namely the underlying meteorological conditions that lead to extreme fire weather events, as well as the spatial connectivity of events in both the Pacific Coast and Four Corners regions. For example, we show that when considering a moving window to define the threshold and mean climate, extreme fire weather events are much drier but not substantially warmer, showing that on short time scales, anomalously low precipitation is more impactful than anomalously high temperatures.

To our knowledge, our study is the first to employ a quantile mapping method to isolate the changes in the mean and variability of the FWI input variables to understand how they individually impact extreme fire weather events. The use of a single model introduces physics-based uncertainties and uncertainties due to climate sensitivities. However, based on analysis in this manuscript (Supplementary Figure 1) and in previous studies, we are confident that the model captures the FWI reasonably well and projects the FWI in the future similarly to other CMIP-style models (Touma et al. 2022; Gallo et al. 2023). Notably, the CESM2-LE allows for the robust estimate of anthropogenically-forced changes in the mean and variability of the individual variables due to the availability of 100 simulations that differ only by internal variability. While our findings show the large impact of increases in the mean of maximum temperatures and decreases in the mean of relative humidity that have been shown in previous studies (Abatzoglou et al. 2019; Jain et al. 2022; Touma et al. 2021), they also show that changes in the variability of relative humidity have a similarly large impact on extreme fire weather event frequency, duration, area, and intensity. In some areas of our study region, the impact of changes in the variability of relative humidity is equal to

that of changes in the mean, doubling the total impact of relative humidity, which is a substantially larger estimate than that of previous studies (e.g., Zhuang et al., 2021). Our findings stress the need to consider changes in the variability as well as the mean of climate variables when understanding climate-change induced changes in different characteristics of extreme climate events, and therefore to employ large ensembles for assessing projections of extreme events.

By using a 35-year moving window that includes all daily values in our quantile-mapping method, we do not differentiate between different timescales of variability – daily to multi-annual timescales are considered together. Previous studies have shown that the El Nino Southern Oscillation (ENSO) and the Pacific Decadal Oscillation (PDO) influence the variability of wildfire occurrence over the pre-industrial and historical period in the western U.S., and that the Atlantic Meridional Oscillation (AMO) can also modulate ENSO's and PDO's influences (Kitzberger et al. 2007). Studies have also shown that ENSO's influence on wildfire danger in the western U.S. is expected to change in future years, as well as the influence on different wildfire-related variables (Fasullo et al., 2018).

## **5. Conclusion**

Our study is one of many that shows that western U.S. wildfire risk is projected to increase over the next century due to increased frequency, persistence and areal coverage of extreme fire weather conditions, and that communities need to plan how to become resilient to these changes. By employing the moving threshold and understanding the role of variability and mean changes in our study, we also begin to shed light on how adaptation measures should be shaped. For instance, our study showed that extreme fire weather events are not only projected to increase in frequency, but also likely to spread over larger areas and become more spatially connected over the coming decades, highlighting the need to prepare for more widespread hazardous conditions. We also found that these changes are not only thermodynamically driven, and that robust and significant changes also occur beyond those that are driven by changes in the mean climate. This finding provides insight into the drivers and predictability of extreme fire weather events on sub-seasonal time scales that are masked when using a fixed threshold (Smith et al. 2025). Our study also shows that by using a large ensemble, we capture the impact of forced changes in the variability of climate variables on extreme fire weather events.

While the use of regionally downscaled (statistically and dynamically) climate projections is important for adaptation policy, they rarely include more than a few realizations and therefore could hide the impacts of the forced changes in climate variability (see Deser et al., 2020 for further reading). One way to overcome this issue is to statistically downscale global ESM large ensembles that are run at relatively coarse resolution or select a few “representative” ensemble members that could capture the forced changes in variability and use those to dynamically downscale climate projections (see, for example, Huang & Swain, 2022). While both pathways will lead to their own uncertainties, we stress the need to capture the impact of anthropogenic forcings on both the variability and mean of our climate system to quantify future risks of extreme fire weather events among other impacts.

#### *Acknowledgments.*

We thank five anonymous reviewers and the editor, Dr. Andrew Hoell, for insightful and constructive feedback. This material is based upon work supported by the NSF National Center for Atmospheric Research, which is a major facility sponsored by the U.S. National Science Foundation under Cooperative Agreement No. 1852977. We would like to acknowledge computing support from the Casper system (<https://ncar.pub/casper>) provided by the NSF National Center for Atmospheric Research (NCAR), sponsored by the National Science Foundation. We also acknowledge the CESM2 Large Ensemble Community Project and supercomputing resources provided by the IBS Center for Climate Physics in South Korea.

#### *Data Availability Statement.*

The CESM2-LE model output is available through <https://www.cesm.ucar.edu/projects/community-projects/LENS2/data-sets.html>. Analysis and visualization scripts will be made available through Zenodo upon publication.

## REFERENCES

Abatzoglou, J., M. Jones, C. Kolden, A. Cullen, M. Sadegh, and E. Williams, 2025: Climate change has increased the odds of extreme regional forest fire years globally, <https://doi.org/10.5194/egusphere-egu25-2594>.

745 Abatzoglou, J. T., 2013: Development of gridded surface meteorological data for ecological  
746 applications and modelling. *Intl Journal of Climatology*, **33**, 121–131,  
747 <https://doi.org/10.1002/joc.3413>.

748 ———, and A. P. Williams, 2016: Impact of anthropogenic climate change on wildfire across  
749 western US forests. *Proc. Natl. Acad. Sci. U.S.A.*, **113**, 11770–11775,  
750 <https://doi.org/10.1073/pnas.1607171113>.

751 ———, ———, and R. Barbero, 2019: Global Emergence of Anthropogenic Climate Change in  
752 Fire Weather Indices. *Geophys. Res. Lett.*, **46**, 326–336,  
753 <https://doi.org/10.1029/2018GL080959>.

754 ———, C. S. Juang, A. P. Williams, C. A. Kolden, and A. L. Westerling, 2021: Increasing  
755 Synchronous Fire Danger in Forests of the Western United States. *Geophysical*  
756 *Research Letters*, **48**, e2020GL091377, <https://doi.org/10.1029/2020GL091377>.

757 Amaya, D. J., and Coauthors, 2023: Marine heatwaves need clear definitions so coastal  
758 communities can adapt. *Nature*, **616**, 29–32, [https://doi.org/10.1038/d41586-023-](https://doi.org/10.1038/d41586-023-00924-2)  
759 [00924-2](https://doi.org/10.1038/d41586-023-00924-2).

760 Andela, N., and Coauthors, 2017: A human-driven decline in global burned area. *Science*,  
761 **356**, 1356–1362, <https://doi.org/10.1126/science.aal4108>.

762 Bui, H. X., Y.-X. Li, and D. Domménget, 2024: Controlling factors of wildfires in Australia  
763 and their changes under global warming. *Environ. Res. Lett.*, **19**, 094030,  
764 <https://doi.org/10.1088/1748-9326/ad69a9>.

765 Burke, M., A. Driscoll, S. Heft-Neal, J. Xue, J. Burney, and M. Wara, 2021: The changing  
766 risk and burden of wildfire in the United States. *Proc. Natl. Acad. Sci. U.S.A.*, **118**,  
767 e2011048118, <https://doi.org/10.1073/pnas.2011048118>.

768 Capotondi, A., and Coauthors, 2024: A global overview of marine heatwaves in a changing  
769 climate. *Commun Earth Environ*, **5**, 701, [https://doi.org/10.1038/s43247-024-01806-](https://doi.org/10.1038/s43247-024-01806-9)  
770 [9](https://doi.org/10.1038/s43247-024-01806-9).

771 Collar, N. M., S. Saxe, B. A. Ebel, K. S. Boden, A. J. Rust, and T. S. Hogue, 2022: Linking  
772 fire-induced evapotranspiration shifts to streamflow magnitude and timing in the  
773 western United States. *Journal of Hydrology*, **612**, 128242,  
774 <https://doi.org/10.1016/j.jhydrol.2022.128242>.

775 Cook, B. I., and R. Seager, 2013: The response of the North American Monsoon to increased  
776 greenhouse gas forcing. *JGR Atmospheres*, **118**, 1690–1699,  
777 <https://doi.org/10.1002/jgrd.50111>.

778 DeRepentigny, P., and Coauthors, 2022: Enhanced simulated early 21st century Arctic sea ice  
779 loss due to CMIP6 biomass burning emissions. *Sci. Adv.*, **8**, eabo2405,  
780 <https://doi.org/10.1126/sciadv.abo2405>.

781 Deser, C., and Coauthors, 2020: Insights from Earth system model initial-condition large  
782 ensembles and future prospects. *Nat. Clim. Chang.*, **10**, 277–286,  
783 <https://doi.org/10.1038/s41558-020-0731-2>.

Deser, C., A. S. Phillips, Michael. A. Alexander, D. J. Amaya, A. Capotondi, M. G. Jacob, and J. D. Scott, 2024: Future Changes in the Intensity and Duration of Marine Heat and Cold Waves: Insights from Coupled Model Initial-Condition Large Ensembles. *Journal of Climate*, **37**, 1877–1902, <https://doi.org/10.1175/JCLI-D-23-0278.1>.

———, W. M. Kim, R. C. J. Wills, I. R. Simpson, S. Yeager, G. Danabasoglu, K. Rodgers, and N. Rosenbloom, 2025: Effects of macro vs. micro initialization and ocean initial-condition memory on the evolution of ensemble spread in the CESM2 large ensemble. *Clim Dyn*, **63**, 62, <https://doi.org/10.1007/s00382-024-07553-z>.

Dowdy, A., G. A. Mills, K. Finkele, and W. De Groot, 2009: *Australian fire weather as represented by the McArthur Forest Fire Danger Index and the Canadian Forest Fire Weather Index*. Centre for Australian Weather and Climate Research.

Fasullo, J. T., 2020: Evaluating simulated climate patterns from the CMIP archives using satellite and reanalysis datasets using the Climate Model Assessment Tool (CMATv1). *Geosci. Model Dev.*, **13**, 3627–3642, <https://doi.org/10.5194/gmd-13-3627-2020>.

Fasullo, J. T., B. L. Otto-Bliesner, and S. Stevenson, 2018: ENSO’s Changing Influence on Temperature, Precipitation, and Wildfire in a Warming Climate. *Geophys. Res. Lett.*, **45**, 9216–9225, <https://doi.org/10.1029/2018GL079022>.

Gallo, C., J. M. Eden, B. Dieppois, I. Drobyshev, P. Z. Fulé, J. San-Miguel-Ayanz, and M. Blackett, 2023: Evaluation of CMIP6 model performances in simulating fire weather spatiotemporal variability on global and regional scales. *Geosci. Model Dev.*, **16**, 3103–3122, <https://doi.org/10.5194/gmd-16-3103-2023>.

Goss, M., D. L. Swain, J. T. Abatzoglou, A. Sarhadi, C. A. Kolden, A. P. Williams, and N. S. Diffenbaugh, 2020: Climate change is increasing the likelihood of extreme autumn wildfire conditions across California. *Environ. Res. Lett.*, **15**, 094016, <https://doi.org/10.1088/1748-9326/ab83a7>.

Hagmann, R. K., and Coauthors, 2021: Evidence for widespread changes in the structure, composition, and fire regimes of western North American forests. *Ecological Applications*, **31**, e02431, <https://doi.org/10.1002/eap.2431>.

Hoell, A., and Coauthors, 2022: Record Low North American Monsoon Rainfall in 2020 Reignites Drought over the American Southwest. *Bull. Amer. Meteor. Soc.*, **103**, S26–S32, <https://doi.org/10.1175/BAMS-D-21-0129.1>.

Huang, X., and D. L. Swain, 2022: Climate change is increasing the risk of a California megaflood. *Sci. Adv.*, **8**, eabq0995, <https://doi.org/10.1126/sciadv.abq0995>.

Jain, P., D. Castellanos-Acuna, S. C. P. Coogan, J. T. Abatzoglou, and M. D. Flannigan, 2022: Observed increases in extreme fire weather driven by atmospheric humidity and temperature. *Nat. Clim. Chang.*, **12**, 63–70, <https://doi.org/10.1038/s41558-021-01224-1>.



822 ———, and Coauthors, 2024: Drivers and Impacts of the Record-Breaking 2023 Wildfire  
823 Season in Canada. *Nat Commun*, **15**, 6764, [https://doi.org/10.1038/s41467-024-](https://doi.org/10.1038/s41467-024-51154-7)  
824 51154-7.

825 Jones, M. W., and Coauthors, 2022: Global and Regional Trends and Drivers of Fire Under  
826 Climate Change. *Reviews of Geophysics*, **60**, e2020RG000726,  
827 <https://doi.org/10.1029/2020RG000726>.

828 ———, and Coauthors, 2024: State of Wildfires 2023–2024. *Earth Syst. Sci. Data*, **16**, 3601–  
829 3685, <https://doi.org/10.5194/essd-16-3601-2024>.

830 Juang, C. S., A. P. Williams, J. T. Abatzoglou, J. K. Balch, M. D. Hurteau, and M. A. Moritz,  
831 2022: Rapid Growth of Large Forest Fires Drives the Exponential Response of  
832 Annual Forest-Fire Area to Aridity in the Western United States. *Geophysical*  
833 *Research Letters*, **49**, e2021GL097131, <https://doi.org/10.1029/2021GL097131>.

834 Kirchmeier-Young, M. C., F. W. Zwiers, N. P. Gillett, and A. J. Cannon, 2017: Attributing  
835 extreme fire risk in Western Canada to human emissions. *Climatic Change*, **144**, 365–  
836 379, <https://doi.org/10.1007/s10584-017-2030-0>.

837 ———, and Coauthors, 2024: Human driven climate change increased the likelihood of the  
838 2023 record area burned in Canada. *npj Clim Atmos Sci*, **7**, 316,  
839 <https://doi.org/10.1038/s41612-024-00841-9>.

840 Kitzberger, T., P. M. Brown, E. K. Heyerdahl, T. W. Swetnam, and T. T. Veblen, 2007:  
841 Contingent Pacific–Atlantic Ocean influence on multicentury wildfire synchrony over  
842 western North America. *Proc. Natl. Acad. Sci. U.S.A.*, **104**, 543–548,  
843 <https://doi.org/10.1073/pnas.0606078104>.

844 Lawrence, A. J., C. Matuch, J. J. Hancock, A. L. Rypel, and L. A. Eliassen, 2022: Potential  
845 Local Extirpation of an Imperiled Freshwater Mussel Population from Wildfire  
846 Runoff. *Western North American Naturalist*, **82**,  
847 <https://doi.org/10.3398/064.082.0405>.

848 Oakley, N. S., 2021: A Warming Climate Adds Complexity to Post-Fire Hydrologic Hazard  
849 Planning. *Earth's Future*, **9**, e2021EF002149, <https://doi.org/10.1029/2021EF002149>.

850 Raymond, C., and Coauthors, 2020: Understanding and managing connected extreme events.  
851 *Nat. Clim. Chang.*, **10**, 611–621, <https://doi.org/10.1038/s41558-020-0790-4>.

852 Rodgers, K. B., and Coauthors, 2021: Ubiquity of human-induced changes in climate  
853 variability. *Earth Syst. Dynam.*, **12**, 1393–1411, [https://doi.org/10.5194/esd-12-1393-](https://doi.org/10.5194/esd-12-1393-2021)  
854 2021.

855 Sharma, A. R., P. Jain, J. T. Abatzoglou, and M. Flannigan, 2022: Persistent Positive  
856 Anomalies in Geopotential Heights Promote Wildfires in Western North America.  
857 *Journal of Climate*, **35**, 6469–6486, <https://doi.org/10.1175/JCLI-D-21-0926.1>.

858 Simpson, I. R., K. A. McKinnon, D. Kennedy, D. M. Lawrence, F. Lehner, and R. Seager,  
859 2024: Observed humidity trends in dry regions contradict climate models. *Proc. Natl.*  
860 *Acad. Sci. U.S.A.*, **121**, e2302480120, <https://doi.org/10.1073/pnas.2302480120>.

861 Skinner, C. B., D. Touma, M. Barlow, D. Singh, and T. King, 2025: The spatial extent of heat  
862 waves has changed over the past four decades. *Commun Earth Environ*, **6**, 662,  
863 <https://doi.org/10.1038/s43247-025-02661-y>.

864 Smith, K. E., and Coauthors, 2025: Baseline matters: Challenges and implications of different  
865 marine heatwave baselines. *Progress in Oceanography*, **231**, 103404,  
866 <https://doi.org/10.1016/j.pocean.2024.103404>.

867 Touma, D., S. Stevenson, F. Lehner, and S. Coats, 2021: Human-driven greenhouse gas and  
868 aerosol emissions cause distinct regional impacts on extreme fire weather. *Nat*  
869 *Commun*, **12**, 212, <https://doi.org/10.1038/s41467-020-20570-w>.

870 ———, ———, D. L. Swain, D. Singh, D. A. Kalashnikov, and X. Huang, 2022: Climate change  
871 increases risk of extreme rainfall following wildfire in the western United States. *Sci.*  
872 *Adv.*, **8**, eabm0320, <https://doi.org/10.1126/sciadv.abm0320>.

873 ———, J. W. Hurrell, M. R. Tye, and K. Dagon, 2023: The Impact of Stratospheric Aerosol  
874 Injection on Extreme Fire Weather Risk. *Earth's Future*, **11**, e2023EF003626,  
875 <https://doi.org/10.1029/2023EF003626>.

876 Van Marle, M. J. E., and Coauthors, 2017: Historic global biomass burning emissions for  
877 CMIP6 (BB4CMIP) based on merging satellite observations with proxies and fire  
878 models (1750–2015). *Geosci. Model Dev.*, **10**, 3329–3357,  
879 <https://doi.org/10.5194/gmd-10-3329-2017>.

880 Virtanen, P., and Coauthors, 2020: SciPy 1.0: fundamental algorithms for scientific  
881 computing in Python. *Nat Methods*, **17**, 261–272, [https://doi.org/10.1038/s41592-019-](https://doi.org/10.1038/s41592-019-0686-2)  
882 [0686-2](https://doi.org/10.1038/s41592-019-0686-2).

883 Vogel, M. M., J. Zscheischler, E. M. Fischer, and S. I. Seneviratne, 2020: Development of  
884 Future Heatwaves for Different Hazard Thresholds. *JGR Atmospheres*, **125**,  
885 e2019JD032070, <https://doi.org/10.1029/2019JD032070>.

886 Van Wagner, C. E., 1987: *Development and structure of the Canadian Forest Fire Weather*  
887 *Index System*. Minister of Supply and Services Canada 37pp.

888 Williams, A. P., and Coauthors, 2022: Growing impact of wildfire on western US water  
889 supply. *Proc. Natl. Acad. Sci. U.S.A.*, **119**, e2114069119,  
890 <https://doi.org/10.1073/pnas.2114069119>.

891 Zhuang, Y., R. Fu, B. D. Santer, R. E. Dickinson, and A. Hall, 2021: Quantifying  
892 contributions of natural variability and anthropogenic forcings on increased fire  
893 weather risk over the western United States. *Proc. Natl. Acad. Sci. U.S.A.*, **118**,  
894 e2111875118, <https://doi.org/10.1073/pnas.2111875118>.

895 Zscheischler, J., and Coauthors, 2020: A typology of compound weather and climate events.  
896 *Nat Rev Earth Environ*, **1**, 333–347, <https://doi.org/10.1038/s43017-020-0060-z>.

897